Multi-mode monitoring and energy management for photovoltaic-storage systems

Darío Benavides[1,2], Paul Arévalo[2,1], Adrián Criollo[2], Marcos Tostado-Véliz[1], and Francisco Jurado[1*]

[1]*Department of Electrical Engineering, University of Jaén, 23700 EPS Linares, Jaén, Spain*

[2]*Department of Electrical Engineering, Electronics, and Telecommunications (DEET), Universidad de Cuenca, Cuenca 010101, Ecuador*

**fjurado@ujaen.es*

Abstract. The integration of photovoltaic generation systems and variable demand can cause instability in the distribution network, due to power fluctuations and the increase in reactants, particularly in the industrial sector. In response, photovoltaic units have been equipped with local storage systems, which eventually absorb power fluctuations and improve installation performance. However, during this procedure other functionalities that energy storage could provide are neglected. Consequently, this study provides a multi-mode energy monitoring and management model that enables voltage regulation, frequency regulation and reactive power compensation through the optimal operation of energy storage systems. With this objective, a smoothing control algorithm is developed that interacts with parameters of the electrical grid at the common connection point and also allows the compensation of reactive power based on an industrial demand profile. This strategy uses the Long short-term memory neural network of historical demand data prior to energy consumption with a relatively low RMSE of 1.2e-09. The results are previously validated in a development environment using a real-time OPAL-RT simulator and tests in the electrical Microgrid laboratory at the University of Cuenca. This configuration allows establishing a demand forecasting model that improves the supervision, automation and analysis of daily energy production. A series of results are provided and analyzed that demonstrate that the new tool allows taking advantage of the provision of multimode functionalities, achieving optimal voltage regulation and improving power quality by reducing the total harmonic distortion THD (V) and THD (I) indices by 0.5. % and 2% respectively.

Keywords: Multi-mode; management; photovoltaic; OPAL-RT; energy storage systems; demand forecast.

Abreviature

EDNs	Electrical distribution networks
ID	Industrial demand
RE	Renewable energies
RES	Renewable energy sources
PV	Photovoltaics
WT	Wind turbine
ESS	Energy storage systems
DG	Distributed generation
MG	Microgrids
SG	Smart grids

BESS	Battery energy storage system
HESS	Hybrid energy storage systems
EMS	Energy management system
CCTI-B	Centro Científico, Tecnológico y de Investigación Balzay
MLPNN	Multilayer perceptron neural network
MTU	Master terminal unit
PSO	Particle swarm optimization
LSTM	Long short-term memory
DRES	Distributed renewable energy sources
SCs	Supercapacitors
RF	Random forest
RRL	Ramp-rate limiter
CI-DRES	Converter-interfaced distributed renewable energy sources
SC	Supercapacitor
LPF	Low pass filter
MA	moving average
P-f	Active Power (P) – frequency (f) Control
Q-v	Reactive Power (Q) – voltage (f) Control
RMSE	Root Mean Squared Error
THD(V)	Total harmonic distortion Voltage
THD(I)	Total harmonic distortion Current

Nomenclature

P_L, Q_L	Active and reactive power of industrial demand with representation of different scenarios
$d(\mathrm{P^{PV}})/dt$	Variation of photovoltaic power in a time t
$d(\mathrm{P^{L}})/dt$	Variation of demand power in a time t
$\mathrm{P_t^{HESS}}$[kW]	Active power supplied by ESS
$\mathrm{P_t^{HESS}}$[kVAr]	Reactive power supplied by ESS
ΔV	Voltage regulation
ΔQ	Reactive power regulation
P_t^{PV}	Power output of the PV system
E_t^{SC}	Energy of a supercapacitor
P_t^{SC}	Power supercapacitor
SOC_t^{SC}	SC state of charge
SOC_t^{VRFB}	VRFB state of charge
$\underline{\mathrm{SOC_t^{VR}}}$	VRFB minimum state of charge
$\overline{\mathrm{SOC_t^{VR}}}$	VRFB maximum state of charge
$\mathrm{P_t^{ref}}$	Reference power value to the storage system
P_t^{VR}	Power VRFB
P_t^L	Active power of industrial demand
Q_t^L	Reactive power of industrial demand
f_t	Output of the Forget Gate
i_t	Output of the Input Gate
o_t	Output of the Output Gate
$\tilde{C}_t$	Candidate version of the new cell state
C_t	Cell state at the current time step
h_t	Output of the LSTM at the current time step
$\mathrm{P_t^{LSTM}}$	Active power demand forecast
$\mathrm{Q_t^{LSTM}}$	Reactive power demand forecast
$\mathrm{Q_t^{VR}}$	Reactive power support from VRFB
$\mathrm{P_t^{VR}}$	Active power support from VRFB

1. Introduction

1.1 Background and motivation

Electrical demand management is essential to optimize electrical distribution networks (EDNs) in modern electrical systems. Due to increasing energy consumption in the industrial sector, it has generated high energy costs for generation and economic dispatch. This problem is especially exacerbated during peak hours of the day, due to the usual working hours of large companies. Every year, industrial demand (DI) increases due to the economic development of cities [1,2]. Therefore, the integration of renewable energies (RE), such as photovoltaics (PV) or wind power (WT) allow the economy to grow in a more sustainable way. The integration of these systems has managed to create more flexible and adaptive electrical grid in distributed generation (DG) with microgrids (MG). However, the uncertainty of renewable resources can cause instability in the electrical system, making the integration of these resources complex. As an alternative to mitigate this impact, energy storage systems (ESS) can be deployed, which can mitigate the instability of the electrical system and ensure a stable and sustainable energy supply. Particularly, this study highlights how leveraging the support of ESS in a multi-objective manner can facilitate a transition towards smart grids (SG) and a more efficient future in modern electrical grids.

The intermittency of renewable energy sourse (RES) in the EDNs can significantly affect power quality. Due to power fluctuations generated by solar and wind resources where their generation depends on factors such as wind and solar irradiation [3–8]. Consequently, power variability with a high rate of change in the power grid can affect the system voltage and frequency [9–13]. In addition, with the integration of inverters/converters from renewable sources, the growth of charging stations for electric vehicles, the gradual increase of electrical machines and power converters in the industrial sector, has increased the consumption of reactive power from the electrical grid. Which also causes voltage imbalances and generation of harmonics that could cause instability in the electrical system [14–16]. In response to the intermittency of RE, the implementation of ESS has made it possible to compensate for this intermittency and minimize the impacts on the electrical grid [3,15,17–19]. These battery-based storage systems can absorb

excess energy during periods of high generation and release it when generation is low. In this way, greater stability is achieved in the power grid and voltage variability and the presence of harmonics are reduced. However, the compensation of reactive power from the demand side has not yet been addressed in a multifunctional way with power smoothing techniques. Therefore, this research studies the specific operation of the ESS that integrates a demand forecasting algorithm that allows smoothing power fluctuations and maintaining the voltage profile in the EDNs through real or reactive power control.

1.2. Literature review

The integration of ESS as power smoothing techniques for RES system has been widely studied [6,20–25]. In recent studies, a novel PV power smoothing method using hybrid energy storage systems (HESS) and machine-learning is proposed in [24] to reduce fluctuations and improve the stability of electrical grids. Similarly, the authors in [26] propose a new power smoothing method using SC to reduce these fluctuations. The method involves two stages: prediction and correction. In [27], is proposed ramp-rate limiter (RRL) control method considers the SC voltage and ensures specific RRL at the distributed renewable energy sources (DRES) connection point without exceeding safety limits. In another study, the combined use of SCs and Battery energy storage system (BESS) is proposed for RRL control in converter-interfaced distributed renewable energy sources (CI-DRES) [28]. The results show that when RR Limitation is activated in both ESS types, the central BESS size can be 40% smaller with a 50% reduction in the BESS converter power. In addition, the long-term impact of power smoothing techniques on BESS capacity degradation is investigated [29]. Different filtering-based algorithms and ramp-rate limitation control schemes are compared. The aging of the BESS is estimated using a rainflow algorithm. RRL control scheme outperforms moving average (MA) and low pass filter (LPF) based methods in terms of achieved smoothing and BESS sizing.

Dimitra Tragianni et al. [30], studied SCs sizing based on comparative study of PV power smoothing methods, comparing two power smoothing algorithms applied to a PV system with BESS. A sizing method based on real irradiation measurements is proposed, indicating the different requirements of each power smoothing method. On the other hand, in [25] proposes a

novel method for power smoothing in WT using a fuzzy-logic-based SC system and time-constant fitting, which addresses the issue of uncertain results and delays in control response. The method generates active power set-point values for the SC to compensate for the intermittency of the WT, and the results were validated through laboratory tests. A two-stage filtering strategy is proposed in [31], control state of charge (SoC) in battery systems, but it still has a delay between input and output. The proposed method, which combines adaptive moving average control (AMAC) and adaptive SoC control (ASC), improves battery utilization and smoothness compared to moving average control (MAC). The effectiveness of the proposed approach is demonstrated in a field experiment. A control strategy that uses energy storage to mitigate rapid voltage variations caused by fluctuations in PV and WT power production has also been studied [32]. The strategy involves using a rule-based RRL control strategy to charge/discharge the energy storage and maintain voltage variations within acceptable limits. The proposed strategy has been tested and validated through simulation, showing that it effectively reduces voltage variations. Whereas in [33], research has focused on RE, particularly PV generation. The storage capacity for PV firming can reach up to 6 kWh for a 600 W system. The storage capacity is analyzed for a system using dynamic PV reference. Experimental verification of a static PV-firming control algorithm is done using a 200 W prototype. The research objectives include integrating batteries into grid-tied power electronics, designing a control method for battery charging and discharging, and developing algorithms for firming the PV output profile.

The implementation of prediction and forecasting algorithms that allow optimizing energy management has been highlighted. In [34] is reported that the industrial sector accounts for 38% of global energy use. Long short-term memory (LSTM) is slightly better than random forest (RF) for load forecasting. The main goal of forecasting is to optimize energy flow and bring financial savings. Smart meters and smart grid technology can help with load management and demand response. The study focused on forecasting the hourly load curve of a meat processing factory. A research group in [35] utilizes a multilayer perceptron neural network (MLPNN) for forecasting solar irradiance, temperature, and load, and particle swarm optimization (PSO) for optimal power flow control. The proposed EMS has a forecasting module for day-ahead prediction and an

optimization module for day-ahead scheduling. The capacity of the PV array is 10 kW, and the battery energy storage capacity is 80 kWh. The EMS is verified on an experimental microgrid, and simulation results demonstrate savings in electricity bill due to optimal energy scheduling. A full-state feedback control strategy for multi-area hydropower systems is proposed in [36]. The integration of redox flow battery (RFB) for non-linear systems is analyzed. In [37], is presented a home energy management system with three effective demand response strategies that are shown to be more effective than other approaches, improving indicators by approximately 70% while only slightly increasing the electricity bill. Some innovative solutions have been proposed in the active control of voltage and frequency in electrical networks. A model predictive controller (MPC) scheme has been proposed to minimize voltage and frequency fluctuations based on Harris Hawks optimization [38]. Where reduced inertia, stochastic load variations and their application in non-linear systems have been favorably evaluated.

[39][24][26][34][40][27][28][29][30][25][31][32][33]Some studies also focus on algorithms that improve the efficiency of investors through exhaustive tests in real-time simulators. The authors in [41] present multiple PV systems and battery energy storage based on bidirectional converter. In which an energy advance feeding component is used, which improves its performance. The tests have been validated with the OPAL-RT real-time controller. Similarly, a hybrid method is proposed, which combines an arithmetic optimization algorithm and particle swarm optimization to improve the efficiency of the inverter through a renewed hysteresis current controller [42]. Real-time simulation allows performance to be analyzed for various scenarios such as solar insolation variation, load alterations and unbalanced non-linear loads [16,43,44]. Besides, a study analyzes the inertia emulation control in which it transforms the behavior of the inverter as a synchronous generator connected to the grid with a battery and SC in the event of power imbalances [45].

1.3. Challenges

Some studies have been presented that integrate the double functionality of active and reactive power compensation based on power smoothing algorithms [3,14–19]. A study discusses the contribution of clients that allow them to receive economic benefits for providing voltage

regulation services through coordinated control of real and reactive power [14]. Active and reactive power flow has also been implemented through a low pass filter (LPF) [15,17]. These studies summarize the importance of applying adaptive techniques to mitigate power fluctuations based on filters, ESS sizing and optimization, state of charge (SoC) control and predictive models. However, the compensation of reactive power and how the voltage at the point of common coupling (PCC) influences is not specifically analyzed. Nor has management been addressed from the demand side, particularly with the reactive power consumed from the grid by the industrial sector and improving the quality of energy in PCC.

After reviewing the current literature, some points of interest in the research have been identified that have not been fully addressed. Whereby, Table 1 presents the key characteristics of the existing literature on PV systems in comparison with the proposed study.

Table 1. Summary of studies related to power smoothing methods, HESS, Reactive power, and Demand management.

Power smoothing methods	Forecasting methods	Use of HESS systems	Simulador / real-time	Experimental validation	Reactive power compensation	Demand management	References
✓		✓	✓	✓			[24,26,27]
✓	✓	✓	✓				[40]
✓	✓	✓		✓		✓	[28,29,46]
	✓		✓		✓		[16]
✓		✓	✓		✓		[47]
		✓	✓		✓	✓	[32,48]
✓		✓	✓				[6,20,45]
			✓	✓	✓		[49]
✓		✓	✓	✓		✓	[12,31,50,51]
✓	✓	✓	✓		✓		[17]
✓		✓	✓	✓	✓		[3,25]
✓	✓		✓		✓	✓	[14]
	✓		✓			✓	[52]
✓	✓	✓	✓	✓	✓	✓	This study

1.4. Contribution and Paper Organization

Unlike to existing literature, we propose in this paper a multi-mode monitoring and energy management strategy for PV-storage systems that aims at leveraging power fluctuations and excess PV energy for compensation of active reactive power in the electrical grid. It also integrates an energy pre-dispatch strategy through a prediction model that allows optimal energy management. In addition, the proposed strategies allow for a notable improvement in power quality in PCC with adequate control of the ESS.

The following points establish the contribution of this article:

- A multimode control method is formulated that allows P-f and Q-V regulation through hybrid storage systems in PV systems based on smoothing techniques.
- An energy pre-dispatch strategy is established for industrial demand profiles under different scenarios using the LSTM neural network.
- A substantial reduction in energy fluctuations and a better balance between energy production and demand is demonstrated with the compensation of active and reactive power in the grid.
- Monitoring the parameters of the electrical grid allows stabilizing the voltage level on PCC, significantly improving power quality with optimal management of reactive power.
- The experimental tests support the discussion of the results in a real-time simulation environment and energy laboratory tests.

The remainder of this paper is organized as follows: Section 2 presents the problem formulation and methodology, Section 3 System modeling through mathematical formulation, Section 4 outlines the multimode management model proposed, Section 5 presents the case study including results and discussions. Finally, section 6 presents the conclusions.

2. Problem statement and methodology

Let us consider an industrial demand profile defined by an active and reactive power consumption (i.e. P_L, Q_L, respectively) with different scenarios during working day hours generally around 8:00 to 18:00, which is connected to a microgrid at a point of common connection that integrates a PV system and ESS. As seen in Fig. 1 (a) and Fig. 1 (b), the electrical distribution requires active and reactive power support to balance demand with generation. This is not completely stocked by the PV generation system. Therefore, it is important to establish demand prediction techniques that allow optimizing energy management.

Besides, in Fig. 1 (c) the percentage of power fluctuation (kW/min) caused by the variation of PV generation $d(\mathrm{P^{PV}})/dt$, variation of demand $d(\mathrm{P^{L}})/dt$, and the result in the power grid have been calculated. These abrupt changes in generation and demand steps can cause instability in the electrical grid [12]. Both, for the variation in the grid frequency (active power) or voltage

variations (reactive power) [47,48]. Hence, a novel control method is generated to mitigate active power fluctuations and reactive power compensation through ESS optimization.

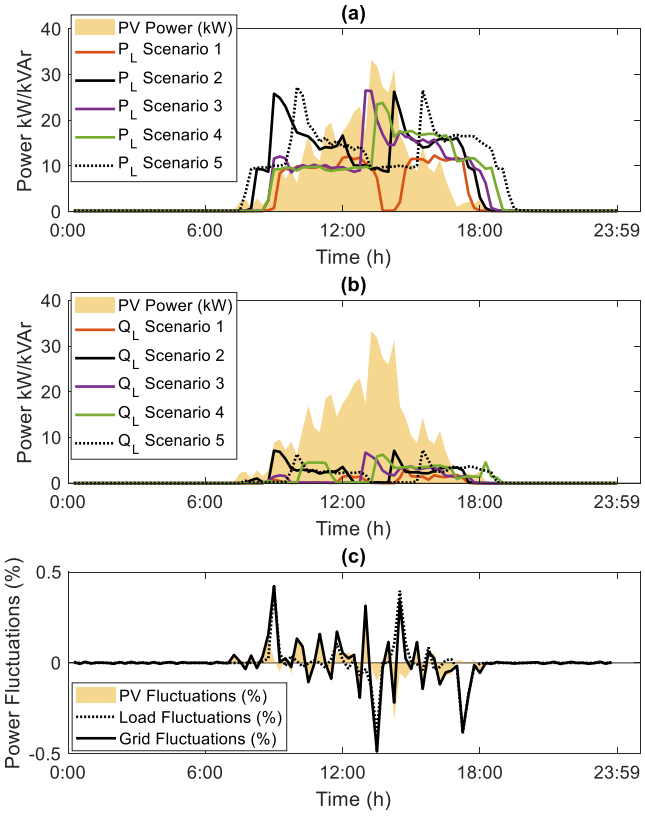

Figure 1. PV power and industrial demand profiles in different scenarios. (a) Active Power required. (b) Reactive Power required. (c) Power fluctuations.

The control methodology is based on the P-f and Q-V control strategies as seen in Fig. 2. Frequency control is regulated through active power control, so Δf is significantly reduced when the rate of change of power is reduced [12]. That is, ΔP is controlled using smoothing techniques, which allows its variability to be reduced over time P_t^{HESS} (kW) [4,6,53]. On the other hand, voltage regulation ΔV at the coupling point can be controlled by regulating the reactive power ΔQ injection to keep it within given limits V_{max} and V_{min} , respectively [3,14,17]. In this case, the new methodology proposes the compensation of reactive power through the storage systems P_t^{HESS} (kvar). In this way, the workflow of the multimode algorithm is proposed, which will be explained in detail in the following sections.

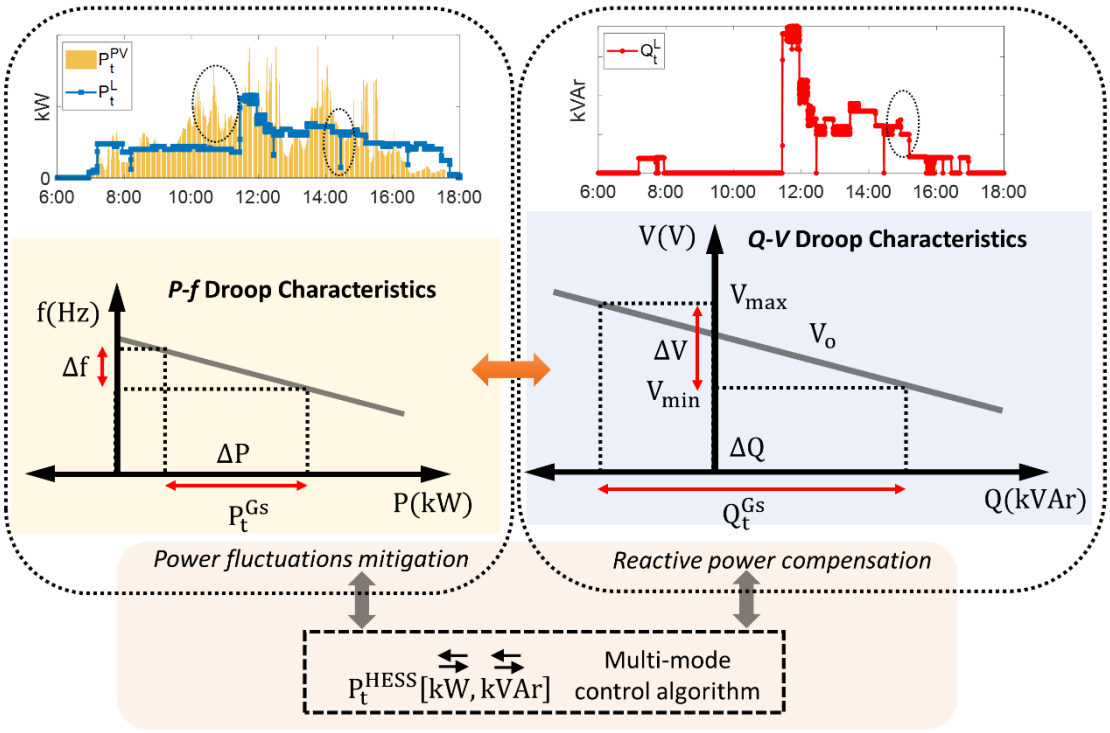

Figure 2. Methodology for multimode control based on P-f and Q-V Droop Characteristics through of power fluctuations mitigation and reactive power compensation.

3. System modelling

The purpose of mathematical modeling is to closely simulate real-world conditions, considering the practical limitations of the laboratory equipment (as presented in the case study later in this document). Experimental tests will be conducted to validate the efficiency, precision, and reliability of the components. The mathematical models will serve as the foundation for computational simulations, enabling the programming of the newly proposed control system. This control system will be integrated with the main control system of the laboratory to transmit reference commands.

3.1. Photovoltaic system

PV generation can be calculated according to (1) as a function of weather parameters [54,55].

$$P_t^{PV} = \gamma_t^{PV}.\lambda^{PV}.\left(\frac{I_{T,t}^{PV}}{I_{S,t}^{PV}}\right).\left[1+\alpha_{pw}^{PV}.\left(T_C^{PV}-T_S^{PV}\right)\right];\ \forall t\ \in T\cup\Xi \qquad (1)$$

where γ_t^{PV} represents the rated capacity of the PV system, λ^{PV} denotes the PV derating factor in percentage, $I_{T,t}^{PV}$ corresponds to the generated PV current, $I_{S,t}^{PV}$ signifies the reverse saturation diode current, α_{pw}^{PV} represents the power temperature coefficient, T_C^{PV} represents the cell temperature,

and T_S^{PV} represents the cell temperature under standard test conditions. The T_C^{PV} values were obtained by measuring with a pyrometer in the laboratory to ensure a more realistic model. In order to ensure the output power of the PV system and prevent any indeterminacy, it is necessary to adhere to the constraints imposed by Eq. (2) [54].

$$\begin{gathered} I_{S,t}^{PV} \neq 0 \\ \alpha_{pw}^{PV}.\left(T_C^{PV} - T_S^{PV}\right) < 1;\ \forall t\ \in T \cup \Xi \end{gathered} \tag{2}$$

3.2. Supercapacitor

The energy stored in a supercapacitor can be determined using (3) [56]:

$$E_t^{SC} = \frac{1}{2}.C^{SC}.(V_t^{SC})^2;\ \forall t\ \in T \cup\ \Xi \tag{3}$$

The efficiency of the supercapacitor, denoted as η_t^{SC}, is determined by the ratio of the useful power, P_t^{SC}, to the total power. The total power accounts for losses and the real power, P_t^{SC}. On the other hand, the state of charge is directly correlated to the equipment's voltage and can be determined using Eq. (4) [57].

$$SOC_t^{SC} = \frac{V_t^{SC} - V_t^{min}}{V_t^{max} - V_t^{min}};\ \forall t\ \in T \cup \Xi \tag{4}$$

where $V_{c,t}^{max};\ V_{c,t}^{min}$ denote the upper and lower voltage limits of the supercapacitor, respectively, observed during its real-time operation. On the other hand, the set of constraints (5) bind variables related to the supercapacitor following rated values [57].

$$\begin{gathered} V_{c,t}^{min} < V_{c,t}^{SC} < V_{c,t}^{max} \\ I_{c,t}^{Ch,max} < I_{c,t}^{SC} < I_{c,t}^{Dis,max};\ \forall t\ \in T, \forall c\ \in C \cup \Xi \end{gathered} \tag{5}$$

where $I_{c,t}^{Ch,max}$ and $I_{c,t}^{Dis,max}$ represent the maximum permissible charge and discharge currents for the SC, respectively.

3.3. Vanadium Redox flow battery

The Vanadium Redox Flow Battery (VRFB) is an electrochemical ESS that utilizes liquid electrolytes for storing electrical energy. It comprises multiple interconnected electrochemical cells arranged in a series configuration, forming a stack. This specific arrangement is critical for

establishing an operational voltage that is suitable for the battery and its associated power electronics. VRFBs store energy through reversible chemical reactions occurring within the electrochemical cells. During the charging process, these reactions alter the ionic state of the electrolyte, leading to a fraction of the electrolyte attaining a higher positive charge compared to the remainder. The resulting electrolyte solutions are known as the positive and negative electrolytes, respectively, and are stored separately in dedicated tanks. Upon discharging, these reactions are reversed, allowing the release of electrical energy for utilization by end users. Continuous circulation of the electrolyte solutions through the stack is maintained during operation. The electrochemical reactions taking place within the stack produce a direct current (DC) output, which can be harnessed for a wide range of applications. VRFBs are capable to undergo regular deep discharges, reaching a charge level of 0%, without incurring any damage to its integrity. Nevertheless, similar to other electrochemical batteries, the output power and capacity of the VRFBs may be influenced by temperature and other operational factors [58].

This paper aims to streamline the model to accurately represent a real-world system while accommodating long-term simulations. To achieve this, established and extensively validated models from the references [59,60] have been taken into account. Hence, the output voltage of the VRFB is computed using (6).

$$V_t^{VRFB} = V_{t,VRFB}^{Stack}\left(SOC_t^{VRFB}, T_t^{VRFB}, \eta_{t,VRFB}^{Cells}\right) + I_{t,VRFB}^{Stack}.R_{VRFB}^{Specific}(T_t^{VRFB}, I_{t,VRFB}^{Stack});\ \forall t \in T \cup \Xi \tag{6}$$

where $V_{t,VRFB}^{Stack}$ represents the stack voltage, $I_{t,VRFB}^{Stack}$ denotes the stack current, and $R_{VRFB}^{Specific}$ is the specific resistance of the VRFB, as shown in (6). It can be observed that the $V_{t,VRFB}^{Stack}$ is dependent on the SOC in the VRFB, temperature, and the number of cells. The stack voltage can be determined by calculating the Nernst equation. To simplify the calculation, the Nernst equation can be defined as a relationship between the open-circuit voltage and the SOC of the VRFB, as said (7) [61].

$$V_{t,VRFB}^{Stack} = \eta_{t,VRFB}^{Cells} \cdot \left\{ V_{VRFB,50\%}^{SOC} + \frac{\Re . T_t^{VRFB}}{F} ln \left[\frac{(SOC_t^{VRFB})^2}{(1-(SOC_t^{VRFB})^2)} \right] \right\};\ \forall t\ \in T \cup \Xi \quad (7)$$

where $\eta_{t,VRFB}^{Cells}$ represents the number of cells in the stack, $V_{VRFB,50\%}^{SOC}$ signifies the open-circuit voltage of a reference cell measured at a 50% state of charge, $\Re$ denotes the molar gas constant (8.314 J/(mol*K)), T_t^{VRFB} represents the process temperature in Kelvin (K), and F represents the Faraday constant (96,485 As/mol). The SOC_t^{VRFB} is defined as the ratio of the currently stored energy to the total energy capacity of the VRFB ($E_{t,VRFB}^{Capacity}$). If the initial SOC_t^{VRFB} is known, its change can be predicted using the following Eq. (8) [61]:

$$SOC_{t,n}^{VRFB} = SOC_t^{VRFB} + \Delta SOC_{t,n-t}^{VRFB}$$
$$SOC_{t,n}^{VRFB} = SOC_t^{VRFB} + \int_t^{t_n} \frac{V_{t,VRFB}^{Stack} \cdot I_{t,VRFB}^{Stack}}{E_{t,VRFB}^{Capacity}} dt;\ \forall t\ \in T \cup \Xi \quad (8)$$

The current flowing through the stack, denoted as $I_{t,VRFB}^{Stack}$, can be calculated by applying Kirchhoff's first law as

$$I_{t,VRFB}^{Stack} = I_{t,VRFB}^{System} - I_{t,VRFB}^{Aux};\ \forall t\ \in T \cup \Xi \quad (9)$$

where $I_{t,VRFB}^{System}$ represents the charging or discharging current provided by the inverter, $I_{t,VRFB}^{Aux}$ denotes the current feeding auxiliary components such as the two pumps, battery controller, installed sensors, and actuators. The inverter governs the battery charging and discharging process. Depending on the power setpoint, the inverter defines the applied DC current system.

The cell stack consists of 12 modules, with minimum and maximum voltages set at 42.7 Vdc and 62.82 Vdc, respectively [62,63]. Once the upper voltage limit is reached, the inverter initiates a current reduction by employing a simple power control loop. The current is limited within the technical specification of the VRFB to ± 200 A-DC on the 48 Vdc bus.

3.4. Utility grid

The mathematical depiction of the electrical grid involves an infinite power generator connected in parallel to the power bus. In order to convey the energy exchanges with the proposed system, the following constraints are stated.

The maximum power limit that the prosumer can procure from the utility grid is subject to the capacity of the grid and the policies of each electric distribution company. Conversely, the following indicates the maximum power limit that the prosumer can export to the utility grid as shown in (10) [37]:

$$\begin{gathered} 0 \leq P_t^{Gd,b} \leq \tau_t^{Gd,b}\overline{p_t{}^{Gdb}} \\ 0 \leq P_t^{Gd,s} \leq \tau_t^{Gd,s}\overline{p_t{}^{Gds}};\ \forall t\ \in T \cup \Xi \end{gathered} \tag{10}$$

Simultaneous bidirectional energy flow between the utility grid and the prosumer is not allowed, as expressed in (11) [37].

$$\tau_t^{Gd,b} + \tau_t^{Gd,s} \leq 1;\ \forall t\ \in T \cup \Xi \tag{11}$$

During outages or grid failures, it is necessary to terminate the power flow between the grid and the prosumer. These constraints are defined as follows:

$$\begin{gathered} \tau_{c,t}^{Gd,b} = O \\ \tau_{c,t}^{Gd,s} = O;\ \forall t\ \in T, \forall c\ \in C \cup \Xi \end{gathered} \tag{12}$$

where $\tau_t^{Gd,b} = 1$ when the grid supplies power to the prosumer, $\tau_t^{Gd,s} = 1$ when the prosumer supplies power to the grid, $p_t{}^{Gdb}$ represents the maximum power flow from the grid to the prosumer, $p_t{}^{Gds}$ represents the maximum power flow from the prosumer to the grid, and 0 refers to the outage scenario matrix.

4. Multi-mode Management Model

This section presents the multimode management model proposed for the grid-connected PV system. On which the use of storage systems is based with a demand prediction strategy. This model is divided into three specific subsections in the analysis of the electrical grid. (a) Obtaining electrical parameters and magnitudes, (b) Demand forecasting algorithm, (c) Multi-mode operation of ESS as seen in the following Fig. 3.

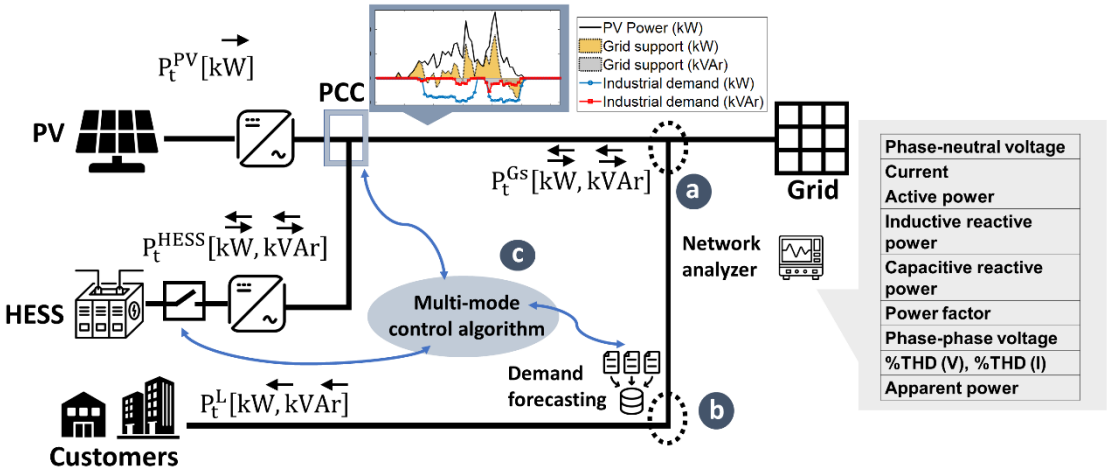

Figure 3. Schematic representation of the proposed multimode model.

4.1. Acquisition architecture for electrical parameters and magnitudes

A Master Terminal Unit (MTU) that has a real-time database with a Hot-StandBy configuration integrates the hardware architecture of the SCADA communications system. The control and automation of the microgrid is carried out by the remote terminal units (RTUs) through the PLCs (Programmer Logic Controller) to each of the application programming interfaces (APIs) of the PV and ESS systems for the control and capture of data [62]. Likewise, network analyzers are responsible for monitoring the electrical parameters and magnitudes of the electrical grid and loads. In parallel, the control of the algorithm is executed in MATLAB through Modbus TCP/IP communication of the same register and writing of variables. In addition, the controller tests are validated through the OPAL-RT real-time simulator, which integrates the modeling of the microgrid previously to obtain the parameters and adjustments. Where the regulation of frequency, voltage at the coupling point and response of the controller in reference power to the ESS is specifically analyzed. The following Fig. 4 presents the configuration of the OPAL-RT real-time simulator and the Microgrid communications architectural scheme.

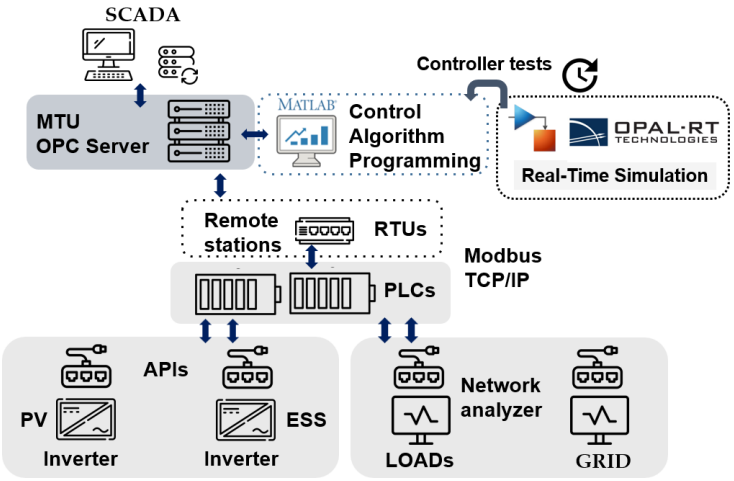

Figure 4. Real-time simulator configuration and Microgrid communications architectural scheme.

4.2. Demand forecasting algorithm

The Long Short-Term Memory (LSTM) neural network is a specialized architecture designed for processing temporal sequences. In the context of predicting industrial demand, this network can be mathematically structured as follows: a temporal sequence of industrial demand data (P_L and Q_L), denoted as $x_1, x_2, \ldots . x_t$, where t represents the current time step. The goal is to predict future demand $\hat{y}_{t+1}$ based on previous observations. Below, each component of an LSTM cell, which is the basic unit of this network, is explained.

To begin, the forget gate f_t determines which information from the previous state C_{t-1} should be discarded $(f_t \approx 0)$ or retained $(f_t \approx 1)$. This decision is based on the concatenation of the previous hidden state h_{t-1} and the current input x_t, passed through a sigmoid function σ as represented in Eq (13). Next, the input gate i_t decides what new information should be added to the state cell. Like the forget gate, it is calculated using a sigmoid function applied to the concatenation of h_{t-1} and x_t, as shown in (14). The output gate o_t determines which part of the current state cell C_t will be used to compute the output. It is calculated using a sigmoid function and the concatenation of h_{t-1} and x_t, as shown in (15) [64–66].

The state cell is updated with a new candidate $\tilde{C}_t$ calculated using the hyperbolic tangent function $tanh$. This candidate reflects the new information that could be added to the state cell, as represented in (16). The state cell is updated by considering both the forget gate and the input gate. C_t represents the updated state cell in (17). Finally, the output h_t, which is the prediction at

time step t, is calculated by considering the output gate and the updated state cell, as seen in (18). In summary, an LSTM cell processes information over time, allowing the network to capture long-term dependencies in temporal sequences, such as observations of industrial demand over time. This learning process enables the network to make accurate predictions about future industrial demand [67–69].

$$f_t = \sigma\left(W_f . [h_{t-1}, x_t] + b_f\right) \tag{13}$$

$$i_t = \sigma(W_i . [h_{t-1}, x_t] + b_i) \tag{14}$$

$$o_t = \sigma(W_o . [h_{t-1}, x_t] + b_o) \tag{15}$$

$$\tilde{C}_t = tanh(W_C . [h_{t-1}, x_t] + b_C) \tag{16}$$

$$C_t = f_t . C_{t-1} + i_t . \tilde{C}_t \tag{17}$$

$$h_t = o_t . tanh(C_t) \tag{18}$$

where, the Forget Gate f_t regulates the amount of past information C_{t-1} to discard, while the Input Gate i_t governs the integration of new information $\tilde{C}_t$ into the cell state C_t. Simultaneously, the Output Gate o_t determines the contribution of the cell state to the output. The Cell Memory Candidate $\tilde{C}_t$ represents a potential new state for the memory cell, and the Cell Memory C_t is the updated state, combining forgotten and new information. The Hidden State h_t is the output, reflecting the current cell state modulated by the Output Gate. These parameters are better summarized in Table 2.

Table 2. LSTM model configuration parameters

Description	Setting
Train-Test Data Split	Train Percentage: 70%
Data Normalization	Range normalization method applied
LSTM Model Architecture	Number of Input Features: Determined by Size of Normalized Training Data
Number of Hidden Units	100
Sequence Length	1
Layers	Sequence Input Layer, LSTM Layer, Fully Connected, Regression Layer
Training Configuration	Optimization Algorithm: Adam
Maximum Epochs	100
Mini-Batch Size	64
Model Training	Training performed using specified layers and options
Prediction Configuration	Number of Predictions: 500
Prediction Loop	Iteration over test data to make predictions
Denormalization	Manual denormalization of predictions using the original data range

4.3. Multi-mode operation of energy storage systems

The multimode management model uses the PV power smoothing algorithm to mitigate the fluctuations generated. In this configuration, SC-based ESSs are used where to obtain the system reference power as described below:

$$P_t^{SC} = \begin{cases} P_t^{ref} - P_t^{PV} & \text{if } \left|\frac{d(P_t^{PV})}{dt}\right| \geq r_{max} \;;\; \forall t \in T \cup \Xi \\ 0 & \text{if } \left|\frac{d(P_t^{PV})}{dt}\right| < r_{max} \;;\; \forall t \in T \cup \Xi \end{cases} \tag{19}$$

$$\left[P_{t-\Delta t}^{PV} - \Delta t \times r_{max}\right] > P_t^{ref} > \left[P_{t-\Delta t}^{PV} + \Delta t \times r_{max}\right] \tag{20}$$

Where the SC power P_t^{SC} is assigned as the difference between the P_t^{ref} and the PV power P_t^{PV} if the value of $\left|\frac{d(P_t^{PV})}{dt}\right|$ exceeds 10%/min of the nominal power of the PV installation r_{max} [8]. Otherwise, the value is zero and does not require use of the SC [26].

In the second strategy, VRFB is used as a demand contribution system with the storage of excess active power from the grid when $P_t^{PV} > P_t^{L}$. On the other hand, it prioritizes the contribution of active and reactive power to the demand directly when $P_t^{L} > P_t^{PV}$.

The active power generated by the PV system is delivered directly to the grid as with the reference power of the HESS. The energy management performed by the controllers makes possible to balance the power flow between sources and demand.

$$P_t^{L} = \begin{cases} P_t^{PV} + P_t^{VR} + P_t^{Gd,s}; \text{ If } P_t^{PV} \geq P_t^{L} \text{ and } \underline{SOC_t^{VR}} < SOC_t^{VR}(k) < \overline{SOC_t^{VR}} \\ P_t^{PV} + P_t^{Gd,s}; \text{ If } P_t^{PV} \geq P_t^{L} \text{ and } SOC_t^{VR}(k) \leq \underline{SOC_t^{VR}} \\ P_t^{VR} + P_t^{Gd,b}; \text{ If } P_t^{PV} < P_t^{L} \text{ and } \underline{SOC_t^{VR}} < SOC_t^{VR}(k) < \overline{SOC_t^{VR}} \\ P_t^{Gd,b}; \text{ If } P_t^{PV} < P_t^{L} \text{ and } SOC_t^{VR}(k) \leq \underline{SOC_t^{VR}} \end{cases} ; \forall t \in T \cup \Xi \tag{21}$$

$$Q_t^{L} = \begin{cases} Q_t^{VR}; \text{ If } \underline{SOC_t^{VR}} < SOC_t^{VR}(k) < \overline{SOC_t^{VR}} \\ Q_t^{Gd,s}; \text{ If } \overline{SOC_t^{VR}} \leq SOC_t^{VR}(k) \leq \underline{SOC_t^{VR}} \end{cases} ; \forall t \in T \cup \Xi \tag{22}$$

Charge and discharge control for VRFBs is prioritized for reactive compensation as follows: $P_t^{VR} = -P_t^{PV}$ If $P_t^{PV} > P_t^{L}$ and $Q_t^{L} = 0$. Likewise with $Q_t^{VR} = Q_t^{L}$ If $Q_t^{L} > 0$.

The following Fig. 5 presents the energy values required for the dispatch of demand under different generation and demand profiles. PV generation is obtained gradually from 6:00 to 18:00

based on a scenario of five representative days. On the other hand, the power of industrial demand corresponds to working hours generally from 8:00 to 18:00. In this case, an analysis is required for the dispatch of active and reactive power for demand Grid support allows energy to be regulated in case of excess generation and supplemented in case of power shortage.

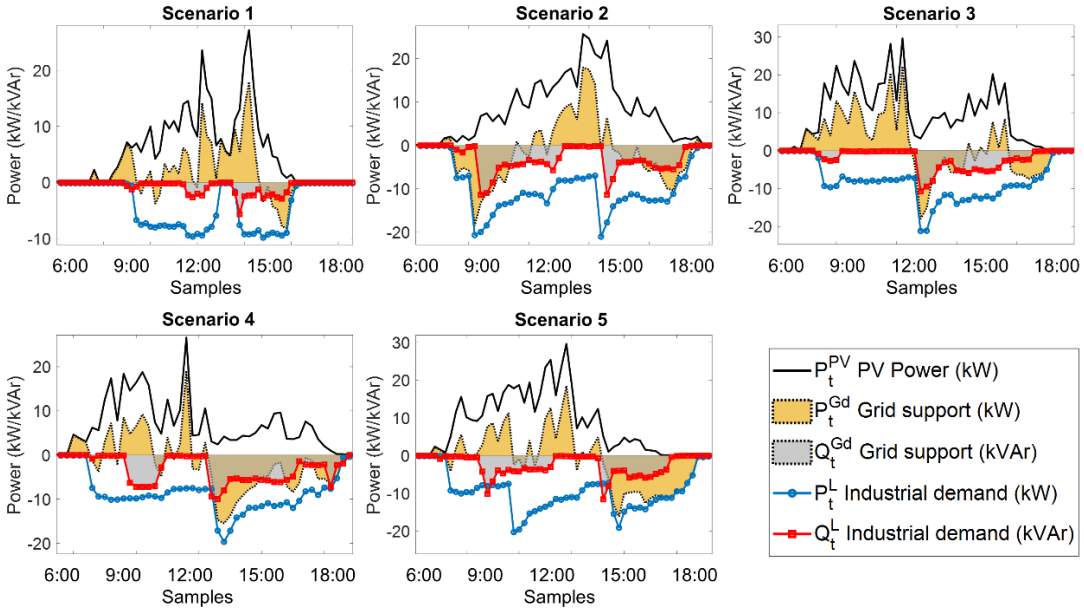

Figure 5. PV generation profiles and industrial demand with support from the grid (Samples – 15 min).

5. Results and Discussion

This section presents the results of the proposed methodology based on the demand forecast, the multimode operation of the control algorithm and Testing and validation of the Controller in real-time Simulator and experimental validation in case study.

5.1. Demand forecasting algorithm

The predictions for P_t^{LSTM} and Q_t^{LSTM} have been generated using LSTM with an impressively low RMSE of 1.2e-09. The model achieved this accuracy within a training time of 00:01:32, utilizing 32,615 samples over 5 epochs. The graphical representation in Fig. 6 illustrates a rapid decline in loss to very low values, accompanied by a simultaneous peak in accuracy.

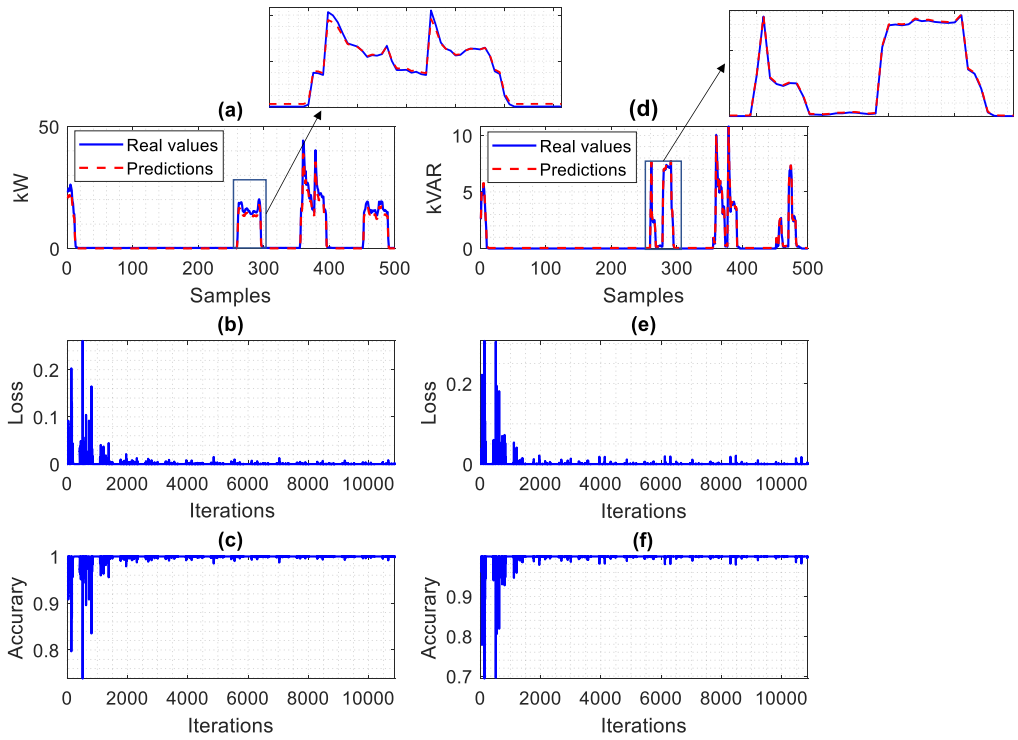

Figure 6. Industrial demand prediction for active power (P) and reactive power (Q) using LSTM. (a), (b), and (c) depict the predictions for active power, while (d), (e), and (f) illustrate the corresponding predictions for reactive power. Each sample in the figures (a) and (d) corresponds to a 15-minute interval in real time.

$$h_t = P_t^{LSTM} + Q_t^{LSTM}$$

5.2. Multi-mode operation of energy storage systems

Figure 7 shows the predispatch values $P_t^{Gd} = P_t^{PV} - P_t^{L}$ based on the prediction using LSTM, where the Q is prioritized for the demand, which will significantly improve the voltage in PCC. Likewise, when excess PV generation P>0 is available, it is stored in the VRFBs to discharge when P<0 is required. In this configuration, the inverters deliver active and reactive power for the discharge of the VRFBs and active power only for the load. The reference power is generated as the active power required from the grid at the connection point with the demand values. The strategy of generating a pre-dispatch allows improving the accumulation of energy for the required hours. Table 3 shows the values of the energy pre-dispatch strategy with demand forecast required for Scenario 2.

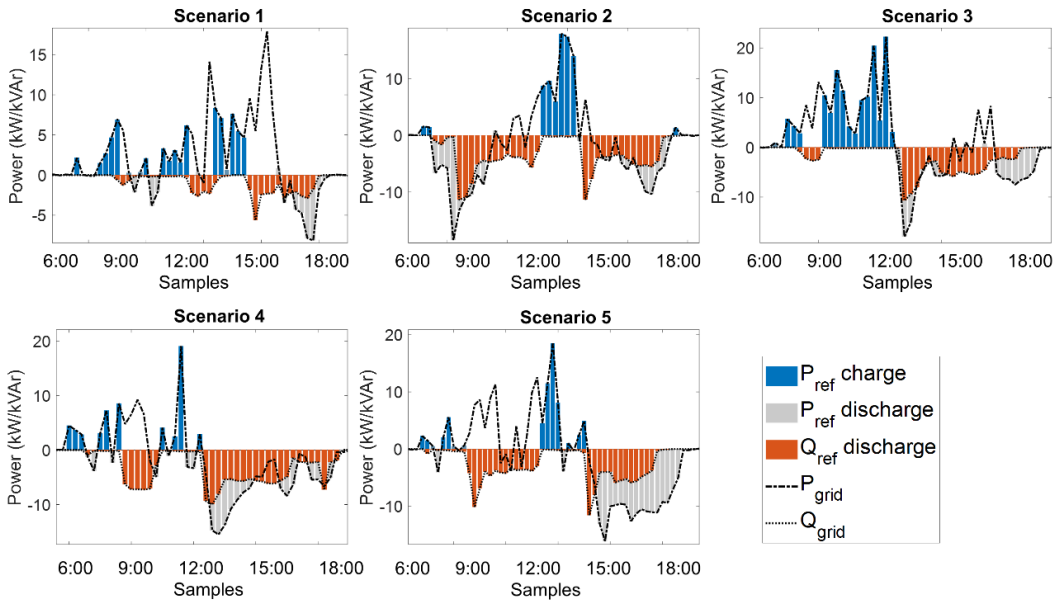

Figure 7. Energy pre-dispatch strategy with demand forecast (Samples – 15 min).

Table 3. Energy pre-dispatch strategy with demand forecast.

Hour	PV Energy [kWh]	Demand (P) [kWh]	Demand (Q) [kVAr]	VRFB/Grid (P) [kWh]	VRFB/Grid (Q) [kVAr]
0:00	0,04	0,06	0,00	-0,02	0,00
1:00	0,05	0,06	0,00	0,00	0,00
2:00	0,05	0,06	0,00	-0,01	0,00
3:00	0,05	0,06	0,00	-0,01	0,00
4:00	0,03	0,06	0,00	-0,03	0,00
5:00	0,05	0,06	0,00	-0,01	0,00
6:00	**0,04**	**0,06**	**0,00**	**-0,02**	**0,00**
7:00	**0,24**	**0,06**	**0,00**	**0,19**	**0,00**
8:00	**0,16**	**0,06**	**0,00**	**0,10**	**0,00**
9:00	**1,89**	**0,13**	**0,11**	**1,76**	**-0,11**
10:00	**2,70**	**3,53**	**0,07**	**-0,82**	**-0,07**
11:00	**2,74**	**3,75**	**0,04**	**-1,01**	**-0,04**
12:00	**4,37**	**3,90**	**0,17**	**0,46**	**-0,17**
13:00	**5,27**	**4,40**	**0,47**	**0,87**	**-0,47**
14:00	**3,89**	**3,32**	**0,03**	**0,57**	**-0,03**
15:00	**2,64**	**0,25**	**0,11**	**2,40**	**-0,11**
16:00	**7,18**	**4,22**	**0,76**	**2,96**	**-0,76**
17:00	**2,61**	**4,39**	**0,50**	**-1,78**	**-0,50**
18:00	**0,74**	**3,69**	**0,44**	**-2,95**	**-0,44**
19:00	0,07	0,13	0,00	-0,06	0,00
20:00	0,03	0,06	0,00	-0,02	0,00
21:00	0,02	0,06	0,00	-0,04	0,00
22:00	0,06	0,06	0,00	0,00	0,00
23:00	0,04	0,06	0,00	-0,02	0,00

5.3. Testing and validation of the controller in real-time simulator

The programming of the controller was carried out in the OPAL-RT real-time simulator with the microgrid models developed in Simulink/MATLAB with the real power profiles obtained

from the SCADA system datalogger and validated in RT-LAB platform. This configuration allowed the controller parameters to be adjusted to validate the results in the PCC. Fig. 8 shows the equipment used during development. In which the OPAL-RT real-time simulator is integrated through a LAN connection to the Local Host. The architecture of the OPAL-RT real-time simulation equipment is made up of the FPGA (Field Programmable Gate Array) that integrates an Intel® Xeon® E3 computer with 4 cores, 3.7 GHz, 16 GB of RAM, 250 GB SSD. This device is responsible for executing the SM Plant subsystem block. While the computer displays the output signals of the SC Scope subsystem independent of the simulation calculation, the characteristics of this device have an Intel(R) Core (TM) i7-10700 CPU processor, 2.90 GHz with 16 Gb RAM. The program runs in Flixed step with the ode5 Dormand-Prince method which evaluates the function six times to calculate the fourth and fifth order solutions and considers the lower one as the error of the solution. In this case, the Computation Burden is subdivided into two processing subsystems and another monitoring subsystem. This reduces the total time involved in the simulated system. Subsystem step size = 0.000050 s (State updated at each local step). In the simulation, a system operation time Ts system= 5e-5 s and switching frequency 20kHz is indicated, which guarantees its operation in a real value environment [43,70]. Likewise, a Ts control = 1e-4 s is assigned for the Voltage Source Converters (VSC) devices integrated into the DC/AC power converters.

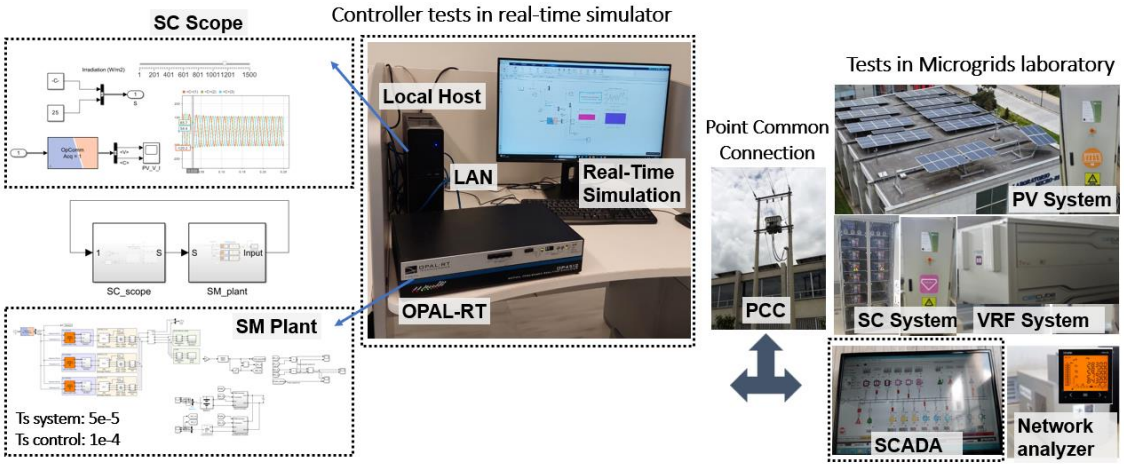

Figure 8. Case study with real-time controller test OPAL-RT and microgrid laboratory tests.

In addition, Fig. 9 presents the results of the configuration of the RT-LAB platform, where two different input profiles are analyzed without the smoothing control Figs. 9 (a-c) and considering the smoothing control Figs. 9 (d-e). A variable input solar irradiation profile produces fluctuations in response of the PV system of 1 to 2.5 kW, with which voltage disturbances can be observed in the PCC waveform. Likewise, the current injected in EDNs depends directly on the PV power. On the other hand, considering the support of the ESS in PCC allows maintaining voltage regulation and improving current variability. In this case, the power is filtered by the smoothing method at a given ramp rate. The difference between the real-time power value and that of the filter is absorbed directly by ESS.

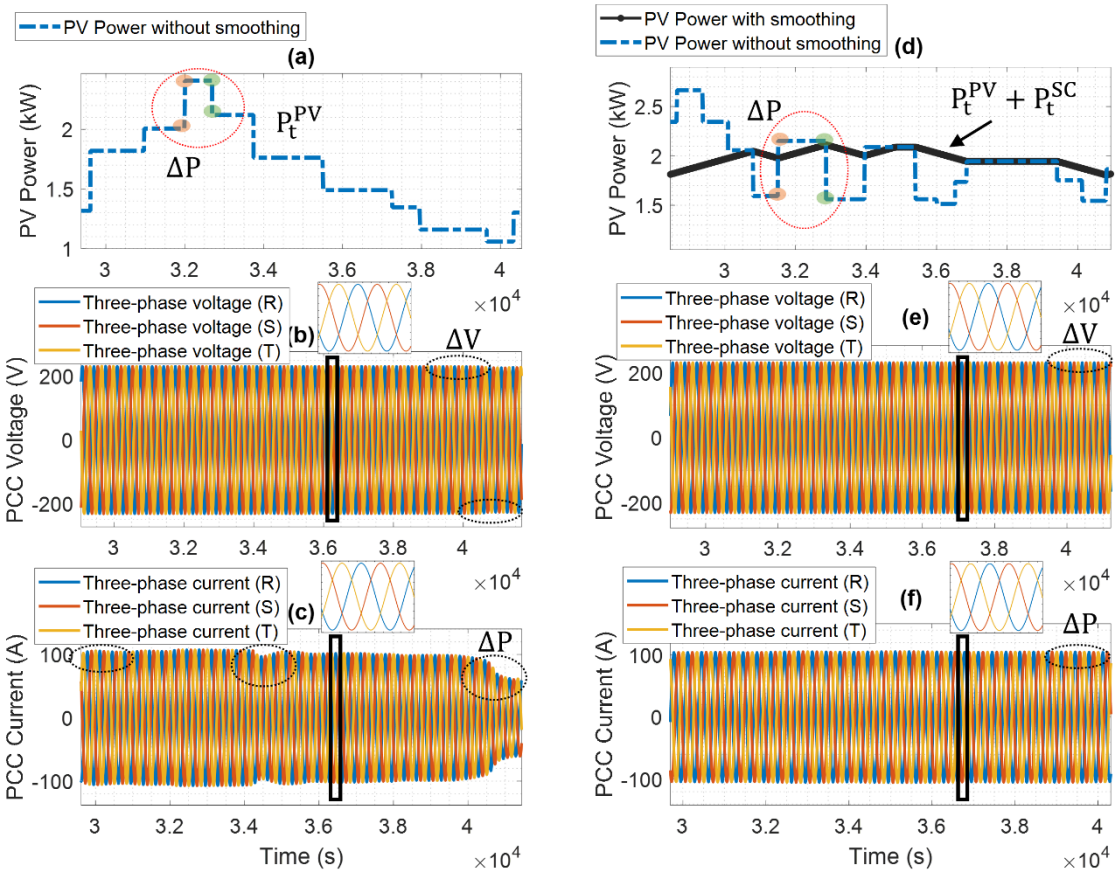

Figure 9. Controller response in OPAL-RT real time simulator: (a) Variable PV power without smoothing. (b) Three-phase voltage measurement without power smoothing. (c) Three-phase Current measurement without power smoothing. (e) Variable PV power with smoothing. (b) Three-phase voltage measurement with power smoothing. (c) Three-phase Current measurement with power smoothing.

In the second phase, the response time of the controller is validated prior to the reference power signal as indicated in (19). As seen in Fig. 10, the real-time P_{ESS} value is directly coupled to the P_{ref} reference value. During the ramp rate of less than $r_{max} \leq \pm 10\%$ of the PV power. The

power adjustment is executed practically in the order of milliseconds. The models used from the Simulink/MATLAB blocks execute the solution of the non-linear systems for the storage systems. The experimental validation of the model shows a maximum error of 5% for the batteries and 2% for the SCs.

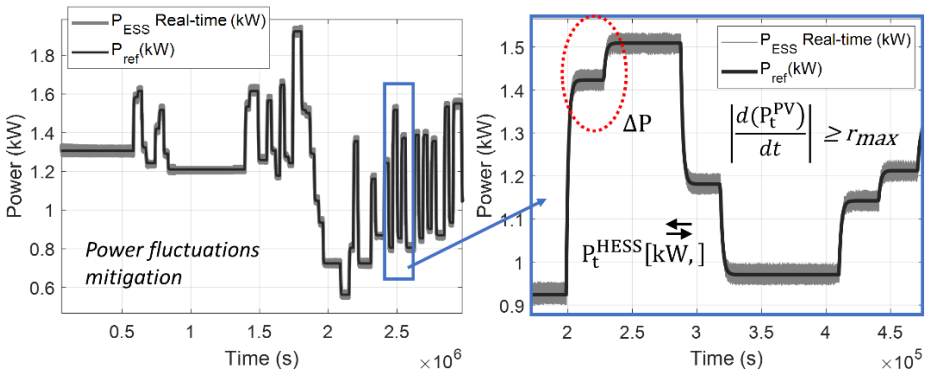

Figure 10. Controller response with Reference power for ESS validated tests with OPAL RT and Simulink/MATLAB.

5.4. Analysis of energy quality indices

Power quality indicators are used to measure the amount of distortion that occurs in the PCC compared to the original signal value. An analysis of the Total Harmonic Distortion (THD) is also presented where the effect of power fluctuations on the voltage THD (V) and current THD (I) are analyzed in Fig. 11 (a) and Fig.11 (b) respectively. It is considered the THD is defined as the root mean square (RMS) value of the total harmonics of the signal, divided by the RMS value of its fundamental signal $I_H = \sqrt{I_2^2 + I_3^2 + \cdots + I_n^2}$. Where I_F RMS value of the fundamental current (similarly for voltage). A reduction in THD(V) < 0.5% and THD (I) < 2% can be seen in Fig. 11 (e) and Fig. 11 (f), respectively. The contribution of the ESS lies in the P-f control through power smoothing and Q-V in the reactive power compensation. Thus, improving the regulation in the PCC of the electrical grid.

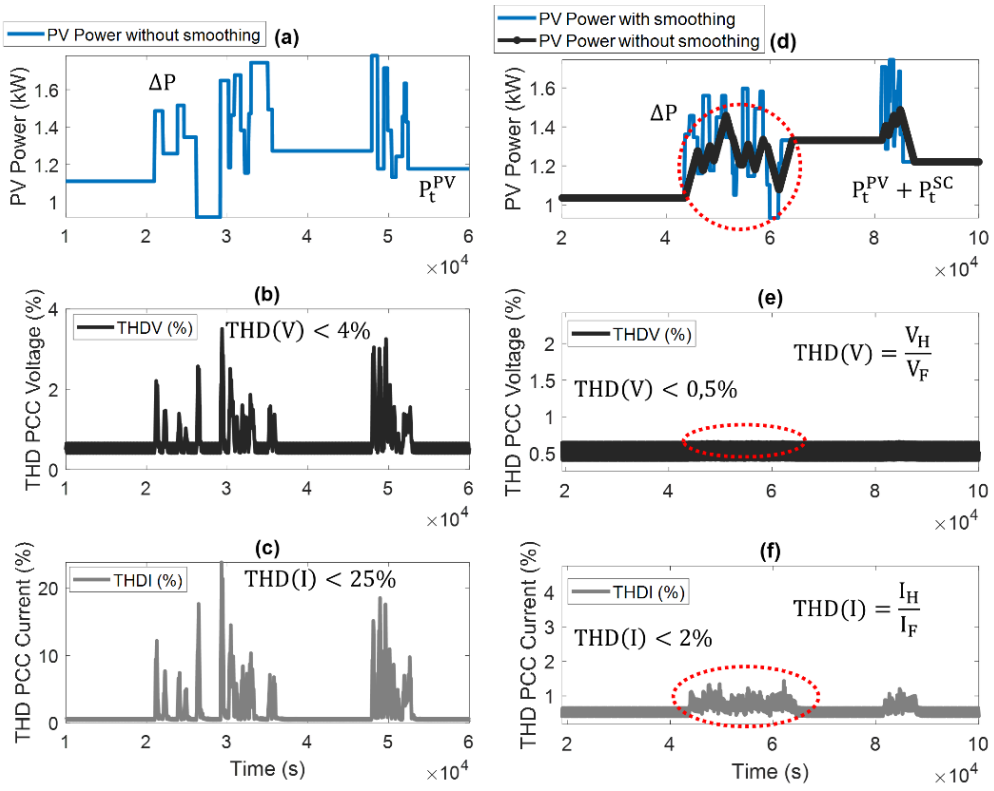

Figure 11. Controller response in OPAL-RT real time simulator: (a) Variable PV power without smoothing. (b) THD Voltage measurement without power smoothing. (c) THD Current measurement without power smoothing. (e) Variable PV power with smoothing. (b) THD Voltage measurement with power smoothing. (c) THD Current measurement with power smoothing.

5.4. Experimental validation in case study

In the experimental validation, the CCTI-B microgrid laboratory has been considered (See Fig. 8) [62]. As presented in Figs. 12 (a-c), an industrial demand profile (kW) is previously assigned. The PV power values (30 kW) are obtained from the SCADA system with which the ESS configuration of the SC (0.4 kWh) and VRFB (100 kWh) directly receive the reference values from the inverters through ModBus communication. The Psc power values absorb and deliver energy to grid minimizing power fluctuations with $r_{max} \leq 10\%$. That is to say, a low ΔP is maintained, so the P-f control strategies are applied to maintain adequate levels of the grid frequency and avoid its instability. On the other hand, Fig. 12 (d) plots the reactive power of industrial demand (kvar). This power is compensated directly by VRFB as a priority in the multimode method. However, it also takes advantage of the support for the demand in active power, that is, covering the demand in $P_t^L > P_t^{PV}$ (See Fig 12 (e)). Finally, Fig. 12 (f) presents

the state of charge of the ESS systems. In this case, the SCs respond only to sudden changes in the steps in the power grid and VRFB contribute active power and reactive power compensation. Which integrates the regulation of voltage in PCC through the Q-V control strategy.

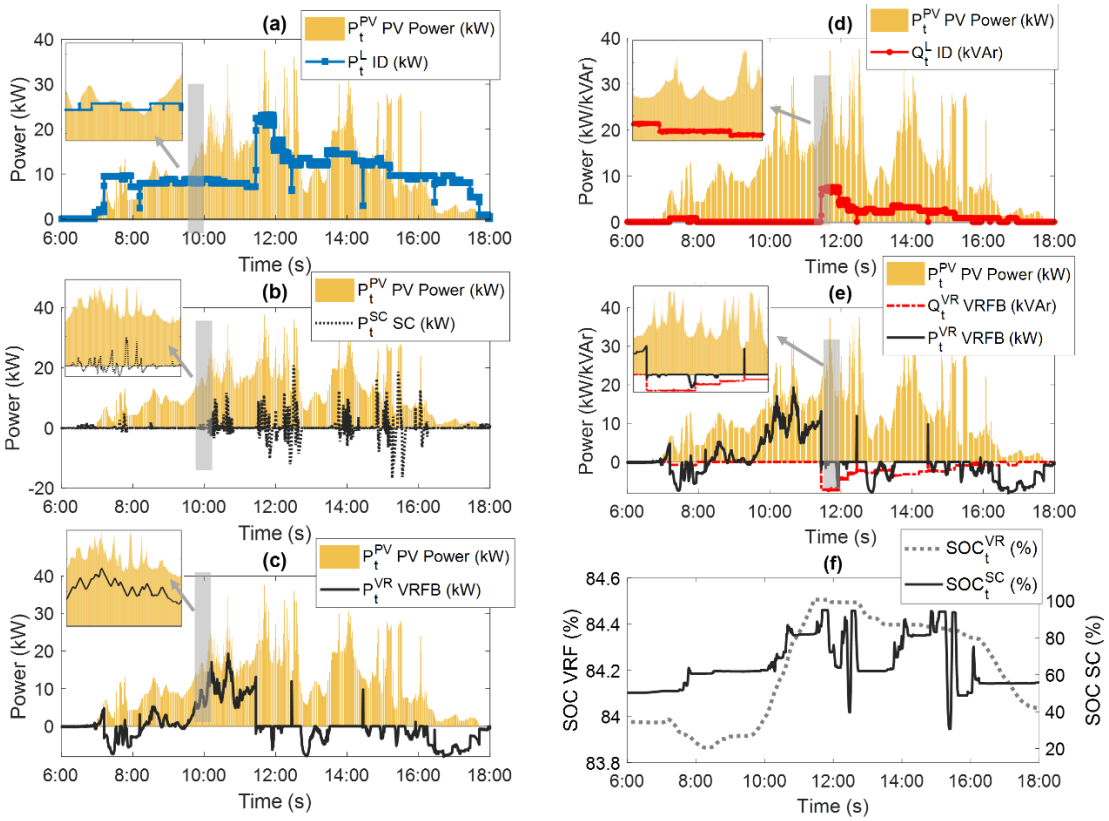

Figure 12. Result of experimental validation in case study: (a) PV power and industrial demand profile active power. (b) SC power supplied and received from the grid. (c) VRFB active power supplied and received from the grid. (d) PV power and industrial demand profile reactive power. (e) VRFB reactive power supplied and received from the grid. (f) SC SOC and VRFB SOC (%).

The results of the operation models based on the ESS are detailed below.

Case 1. Active and reactive power support with Load fluctuation: in this activity there is an increase in the load in active and reactive power, which is managed by the PV power and VRFB, as there are no PV Power fluctuations the use is not required of SC.

Case 2. Active and reactive power support with PV fluctuation: if PV fluctuations occur, the SCs absorb the excess energy and deliver energy to the grid if the ramp limit is exceeded. On the other hand, if active and reactive power is required from the load, the VRFBs fulfill this function. It is important to clarify that when charging VRFBs, only delivery of active or reactive power at the same time or discharge of active or reactive power is allowed. That is, it does not allow charging with active power and discharging reactive power at the same time, due to the

flow of the inverter with the grid. Therefore, this limitation has also been considered in the algorithm.

Case 3: Active power support with PV fluctuation: The operation of the SC allows the control of PV fluctuations, consequently, the SCs only interact with the grid if there is an increase in the ramp rate exceeding the maximum pre-established value ($r_{max} \geq \pm 10\%$). In different values its operation is null. Besides, if there is no reactive load from the demand, the VRFBs take advantage of the surplus energy for future operations.

Case 4: Active and reactive power support with PV and Load Fluctuation. When power variations occur in the load with active and reactive power, the VRFBs have functionality combined with the energy requirement. On the other hand, SCs allow their hydride interaction if required. In Fig 13. The different types of operations indicated above are graphed.

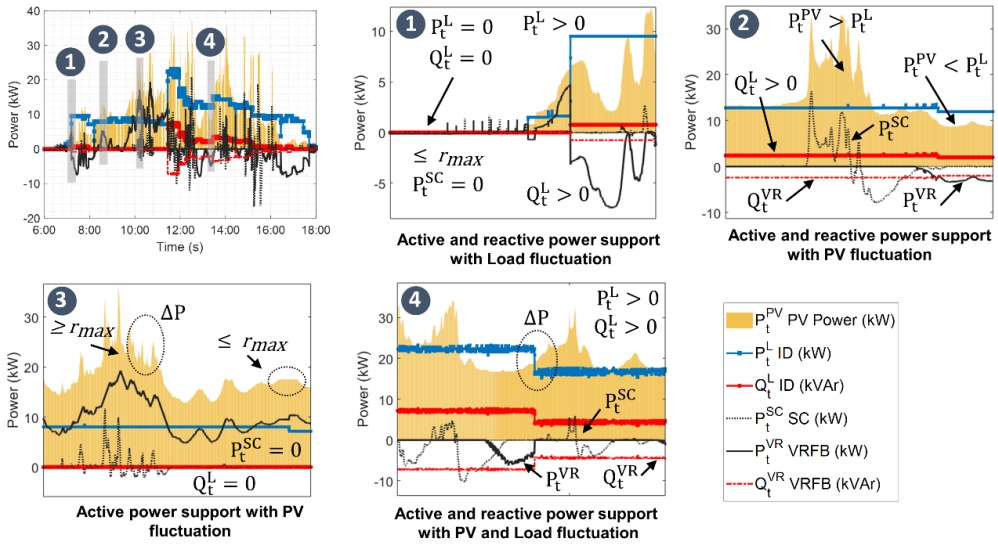

Figure 13. Results of the energy monitoring and management algorithm of the ESS operating modes.

After the application of the management algorithm, the results are analyzed in the PCC based on the compensation of active and reactive power. Fig. 14 shows the voltage values of the three-phase system (R-S-T) with respect to the neutral measured directly at the PCC. Two scenarios based on PV production without ESS integration in the grid and with ESS coupling of the proposed multimode method have been considered. As can be seen, the reactive power compensation at the coupling point significantly improves voltage regulation by reducing the ΔV.

In addition, during working hours from 6:00 to 18:00, VRFB's reactive compensation offers optimal regulation around 127 Vac.

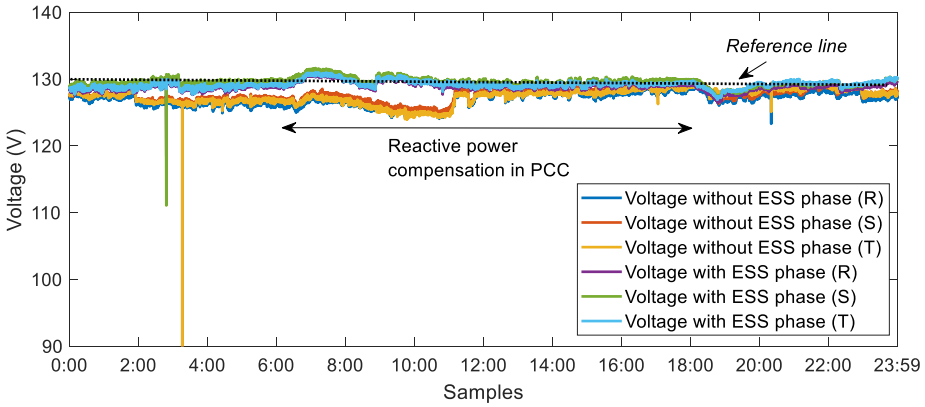

Figure 14. Voltage regulation adjustment in PCC three-phase voltage measurement.

Figure 15 presents the fitting results in the PCC with the average voltage measurements through the normal distribution function. Fig. 15 (a) shows the voltage drop over the number of events over 3×10^4 and a voltage drop range 4 V from the nominal value. On the other hand, in Fig. 15 (b) the measurement of events with the proposed controller improves significantly in a 2 V range in PCC with the grid. Finally, the Empirical cumulative distribution function of the Δ Voltage PCC does not support ESS (- 4 V to 4 V) and with ESS support (- 2 V to 4 V) respectively.

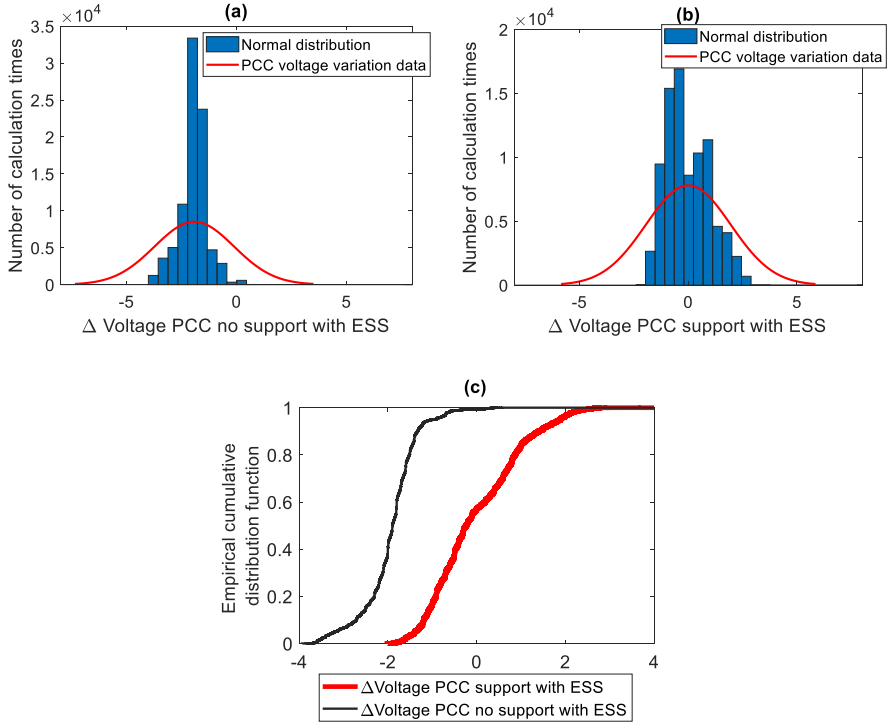

Figure 15. Normal distribution function as voltage regulation in PCC: (a) Analysis without controller (b) Analysis with controller of the proposed method. (c) Empirical cumulative distribution function.

6. Conclusions

This paper presents an innovative multi-mode prediction and optimization strategy to mitigate power fluctuations in a photovoltaic system with vanadium redox flow battery storage and supercapacitors. The proposed system allows multimode operation through P-f and Q-V control strategies that regulate power fluctuations and allow reactive power compensation. In this way, the optimization of energy dispatch processes, frequency regulation, regulation of power fluctuations, voltage regulation in the PCC, compensation of reactive power and reduction of THD indices are covered. The implementation of a multimode monitoring and management model successfully tackles the intermittent nature of photovoltaic resources, enhancing the distribution grid's stability.

The results showcase the effectiveness of various components, starting with the LSTM-based demand forecasting algorithm, demonstrating impressive precision with an RMSE of 1.2e-09. The multimode operation of ESS is highlighted, emphasizing a pre-dispatch strategy that prioritizes demand and utilizes VRFB batteries to store and release energy as needed. This is evident in the pre-dispatch values for different hours, optimizing energy accumulation.

Using the proposed method, a reduction of THD (V) < 0.5% and THD (I) < 2% has been achieved for grid-connected PV systems. Which allows us to offer advantages to reduce the impact of the integration of renewable energies progressively.

Encouraging outcomes are observed in real-time simulator validation and experimental validation in the microgrid laboratory. Real-time validation underscores the importance of smoothing control, revealing that without it, solar power fluctuations lead to significant disturbances, while with smoothing control, voltage regulation is maintained, and current variability is improved.

Acknowledgments

The authors wish to thank to the Spanish Ministry of Science and Innovation and European Union NextGenerationEU/PRTR, under the research Project “Desarrollo de herramientas computacionales para microrredes multi-energía con vectores de electricidad, hidrógeno y gas” (TED2021-129631B-C31).

The author Paul Arévalo thanks the Call for Grants for the Requalification of the Spanish University System for 2021-2023, Margarita Salas Grants for the training of young doctors awarded by the Ministry of Universities and financed by the European Union –Next Generation EU.

The authors thank Universidad de Cuenca for easing access to the facilities of the Microgrid Laboratory of the Centro Científico Tecnológico y de Investigación Balzay (CCTI-B), for allowing the use of its equipment, and for authorizing its staff the provision of technical support necessary to carry out the experiments described in this paper.

References

[1] Marques AC, Fuinhas JA, Tomás C. Energy efficiency and sustainable growth in industrial sectors in European Union countries: A nonlinear ARDL approach. J Clean Prod 2019;239:118045. https://doi.org/10.1016/J.JCLEPRO.2019.118045.

[2] Caballero V, Briones A, Coca-Ortegón A, Pérez A, Barrios B, de la Mano M. Analysis and simulation of an Urban-Industrial Sustainable Energy Community: A use case in San Juan de Mozarrifar using photovoltaic energy. Energy Reports 2023;9:1589–605. https://doi.org/10.1016/J.EGYR.2022.12.059.

[3] Somayajula D, Crow M. An integrated active power filter-ultracapacitor design to provide intermittency smoothing and reactive power support to the distribution grid 2015:1–1. https://doi.org/10.1109/PESGM.2015.7286067.

[4] Shivashankar S, Mekhilef S, Mokhlis H, Karimi M. Mitigating methods of power fluctuation of photovoltaic (PV) sources - A review. Renewable and Sustainable Energy Reviews 2016;59:1170–84. https://doi.org/10.1016/J.RSER.2016.01.059.

[5] Gu FC, Chen HC. Modelling and control of vanadium redox flow battery for smoothing wind power fluctuation. IET Renewable Power Generation 2021;15:3552–63. https://doi.org/10.1049/RPG2.12244.

[6] Sukumar S, Marsadek M, Agileswari KR, Mokhlis H. Ramp-rate control smoothing methods to control output power fluctuations from solar photovoltaic (PV) sources—A review. J Energy Storage 2018;20:218–29. https://doi.org/10.1016/J.EST.2018.09.013.

[7] Jiang Q, Hong H. Wavelet-based capacity configuration and coordinated control of hybrid energy storage system for smoothing out wind power fluctuations. IEEE Transactions on Power Systems 2013;28:1363–72. https://doi.org/10.1109/TPWRS.2012.2212252.

[8] Vahan G, Booth S. Review of PREPA technical requirements for interconnecting wind and solar generation. National Renewable Energy Laboratory (NREL), Tech Rep NREL/TP-5D00-57089 2013:72. https://doi.org/10.1136/jcp.22.4.417.

[9] Eto JH, Undrill J, Roberts C, Mackin P, Ellis J. Frequency Control Requirements for Reliable Interconnection Frequency Response 2018.

[10] Kerdphol T, Rahman FS, Watanabe M, Mitani Y. Robust Virtual Inertia Control of a Low Inertia Microgrid Considering Frequency Measurement Effects. IEEE Access 2019;7:57550–60. https://doi.org/10.1109/ACCESS.2019.2913042.

[11] Lu N, Fang J, Tang Y, Hredzak B. A Frequency Deadband-Based Virtual Inertia Control for Grid-Connected Power Converters. ICPE 2019 - ECCE Asia - 10th International Conference on Power Electronics - ECCE Asia 2019. https://doi.org/10.23919/ICPE2019-ECCEASIA42246.2019.8796992.

[12] Criollo A, Minchala-Avila LI, Benavides D, Arévalo P, Tostado-Véliz M, Sánchez-Lozano D, et al. Enhancing Virtual Inertia Control in Microgrids: A Novel Frequency Response Model Based on Storage Systems. Batteries 2024, Vol 10, Page 18 2024;10:18. https://doi.org/10.3390/BATTERIES10010018.

[13] Huang X, Wang K, Li G. Virtual Inertia Based Control of Two-stage Photovoltaic Inverters for Frequency Regulation in Islanded Micro-grid. IEEE Power and Energy Society General Meeting 2018;2018-August. https://doi.org/10.1109/PESGM.2018.8586544.

[14] Yang J, Tushar W, Saha TK, Alam MR, Li Y. Prosumer-Driven Voltage Regulation via Coordinated Real and Reactive Power Control. IEEE Trans Smart Grid 2022;13:1441–52. https://doi.org/10.1109/TSG.2021.3125339.

[15] Shin SS, Oh JS, Jang SH, Cha JH, Kim JE. Active and Reactive Power Control of ESS in Distribution System for Improvement of Power Smoothing Control. Journal of Electrical Engineering and Technology 2017;12:1007–15. https://doi.org/10.5370/JEET.2017.12.3.1007.

[16] Gira N, Dahiya AK. ANFIS Controlled Reactive Power Compensation Utilizing Grid-Connected Solar Photovoltaic System as PV-STATCOM. J Sci Ind Res (India) 2021;80:668–74. https://doi.org/10.56042/JSIR.V80I08.46922.

[17] Gao JT, Shih CH, Lee CW, Lo KY. An Active and Reactive Power Controller for Battery Energy Storage System in Microgrids. IEEE Access 2022;10:10490–9. https://doi.org/10.1109/ACCESS.2022.3145009.

[18] Hu J, Ye C, Ding Y, Tang J, Liu S. A Distributed MPC to Exploit Reactive Power V2G for Real-Time Voltage Regulation in Distribution Networks. IEEE Trans Smart Grid 2022;13:576–88. https://doi.org/10.1109/TSG.2021.3109453.

[19] Golshannavaz S. Cooperation of electric vehicle and energy storage in reactive power compensation: An optimal home energy management system considering PV presence. Sustain Cities Soc 2018;39:317–25. https://doi.org/10.1016/J.SCS.2018.02.018.

[20] Li X, Hui D, Lai X. Battery energy storage station (BESS)-based smoothing control of photovoltaic (PV) and wind power generation fluctuations. IEEE Trans Sustain Energy 2013;4:464–73. https://doi.org/10.1109/TSTE.2013.2247428.

[21] Raoofat M, Saad M, Lefebvre S, Asber D, Mehrjedri H, Lenoir L. Wind power smoothing using demand response of electric vehicles. International Journal of Electrical Power & Energy Systems 2018;99:164–74. https://doi.org/10.1016/J.IJEPES.2017.12.017.

[22] Ina N, Yanagawa S, Kato T, Suzuoki Y. Smoothing of PV system output by tuning MPPT control. Electrical Engineering in Japan 2005;152:10–7. https://doi.org/10.1002/eej.20106.

[23] Wang G, Ciobotaru M, Agelidis VG. Power Smoothing of Large Solar PV Plant Using Hybrid Energy Storage. IEEE Trans Sustain Energy 2014;5:834–42. https://doi.org/10.1109/TSTE.2014.2305433.

[24] Arévalo P, Benavides D, Tostado-Véliz M, Aguado JA, Jurado F. Smart monitoring method for photovoltaic systems and failure control based on power smoothing techniques. Renew Energy 2023;205:366–83. https://doi.org/10.1016/J.RENENE.2023.01.059.

[25] Ochoa D, Martinez S, Arévalo P. A Novel Fuzzy-Logic-Based Control Strategy for Power Smoothing in High-Wind Penetrated Power Systems and Its Validation in a Microgrid Lab. Electronics 2023, Vol 12, Page 1721 2023;12:1721. https://doi.org/10.3390/ELECTRONICS12071721.

[26] Benavides D, Arévalo P, Aguado JA, Jurado F. Experimental validation of a novel power smoothing method for on-grid photovoltaic systems using supercapacitors. International Journal of Electrical Power & Energy Systems 2023;149:109050. https://doi.org/10.1016/J.IJEPES.2023.109050.

[27] Malamaki KND, Casado-Machado F, Barragan-Villarejo M, Gross AM, Kryonidis GC, Martinez-Ramos JL, et al. Ramp-rate control of DRES employing supercapacitors in distribution systems. SEST 2021 - 4th International Conference on Smart Energy Systems and Technologies 2021. https://doi.org/10.1109/SEST50973.2021.9543116.

[28] Dimoulias SC, Malamaki KND, Gross AM, De Paula Garcia-Lopez F, Kryonidis GC, Barragan-Villarejo M. Ramp-Rate Limitation of Renewable Energy Sources for Voltage Quality Improvement in Distribution Networks: An Experimental Study. 2023 International Conference on Smart Energy Systems and Technologies, SEST 2023 2023. https://doi.org/10.1109/SEST57387.2023.10257447.

[29] Malamaki KND, Fu A, Mauricio JM, Cvetković M, Demoulias CS. Evaluation of Ramp-Rate Limitation at Distribution Transformer Level via Central and Distributed Storage Systems. 2023 IEEE Belgrade PowerTech, PowerTech 2023 2023. https://doi.org/10.1109/POWERTECH55446.2023.10202995.

[30] Dimitra Tragianni S, Oureilidis KO, Demoulias CS. Supercapacitor sizing based on comparative study of PV power smoothing methods. 2017 52nd International Universities Power Engineering Conference, UPEC 2017 2017;2017-Janua:1–6. https://doi.org/10.1109/UPEC.2017.8232029.

[31] Kini R, Raker D, Stuart T, Ellingson R, Heben M, Khanna R. Mitigation of PV Variability Using Adaptive Moving Average Control. IEEE Trans Sustain Energy 2020;11:2252–62. https://doi.org/10.1109/TSTE.2019.2953643.

[32] Alam MJE, Muttaqi KM, Sutanto D. Battery Energy Storage to Mitigate Rapid Voltage/Power Fluctuations in Power Grids Due to Fast Variations of Solar/Wind Outputs. IEEE Access 2021;9:12191–202. https://doi.org/10.1109/ACCESS.2021.3051283.

[33] Alharbi M, Batarseh I. A novel approach and analysis for PV firming using grid-tied three-port microinverter. J Curr Sci Technol 2020;10:1–19. https://doi.org/10.14456/jcst.2020.1.

[34] Ungureanu S, Topa V, Cziker A. Industrial load forecasting using machine learning in the context of smart grid. 2019 54th International Universities Power Engineering Conference, UPEC 2019 - Proceedings 2019:1–6. https://doi.org/10.1109/UPEC.2019.8893540.

[35] Tayab UB, Yang F, El-Hendawi M, Lu J. Energy management system for a grid-connected microgrid with photovoltaic and battery energy storage system. ANZCC 2018 -

2018 Australian and New Zealand Control Conference 2018:141–4. https://doi.org/10.1109/ANZCC.2018.8606557.

[36] Rangi S, Jain S, Arya Y. Utilization of energy storage devices with optimal controller for multi-area hydro-hydro power system under deregulated environment. Sustainable Energy Technologies and Assessments 2022;52:102191. https://doi.org/10.1016/J.SETA.2022.102191.

[37] Tostado-Véliz M, Arévalo P, Kamel S, Zawbaa HM, Jurado F. Home energy management system considering effective demand response strategies and uncertainties. Energy Reports 2022;8:5256–71. https://doi.org/10.1016/j.egyr.2022.04.006.

[38] Kumar V, Sharma V, Arya Y, Naresh R, Singh A. Stochastic wind energy integrated multi source power system control via a novel model predictive controller based on Harris Hawks optimization. Energy Sources, Part A: Recovery, Utilization, and Environmental Effects 2022;44:10694–719. https://doi.org/10.1080/15567036.2022.2156637.

[39] Elmorshedy MF, Elkadeem MR, Kotb KM, Taha IBM, Mazzeo D. Optimal design and energy management of an isolated fully renewable energy system integrating batteries and supercapacitors. Energy Convers Manag 2021;245:114584. https://doi.org/10.1016/j.enconman.2021.114584.

[40] Fregosi D, Pilot N, Bolen M, Hobbs WB. An Analysis of Storage Requirements and Benefits of Short-Term Forecasting for PV Ramp Rate Mitigation. IEEE J Photovolt 2023;13:315–24. https://doi.org/10.1109/JPHOTOV.2022.3231713.

[41] Chauhan S, Singh B. Control of Three-Phase Grid Integrated Multiple Solar Photovoltaic Arrays-BES Based MG. IEEE Trans Ind Appl 2021;57:6167–81. https://doi.org/10.1109/TIA.2021.3109843.

[42] Mohapatra B, Sahu BK, Pati S. Power Quality Alleviation of a Grid-Integrated Photovoltaic System Based on Novel Meta-Heuristic Optimization Technique Using OPAL-RT Real-Time Platform. Electrica 2023. https://doi.org/10.5152/ELECTRICA.2023.0199.

[43] Chauhan S, Singh B. Utility intertie multi-photovoltaic-inverters-based microgrid control for solar rooftop. IET Energy Systems Integration 2022;4:247–66. https://doi.org/10.1049/ESI2.12058.

[44] Ismeil MA, Alfouly A, Hussein HS, Hamdan I. Hardware in the Loop Real-Time Simulation of Improving Hosting Capacity in Photovoltaic Systems Distribution Grid With Passive Filtering Using OPAL-RT. IEEE Access 2023;11:78119–34. https://doi.org/10.1109/ACCESS.2023.3298547.

[45] Sarojini RK, Palanisamy K, Sanjeevikumar P, Nielsen JBH. Inertia emulation control technique based frequency control of grid-connected single-phase rooftop photovoltaic system with battery and supercapacitor. IET Renewable Power Generation 2020;14:1156–63. https://doi.org/10.1049/IET-RPG.2019.0873.

[46] Reihani E, Motalleb M, Ghorbani R, Saad Saoud L. Load peak shaving and power smoothing of a distribution grid with high renewable energy penetration. Renew Energy 2016;86:1372–9. https://doi.org/10.1016/J.RENENE.2015.09.050.

[47] Shin SS, Oh JS, Jang SH, Cha JH, Kim JE. Active and Reactive Power Control of ESS in Distribution System for Improvement of Power Smoothing Control. Journal of Electrical Engineering and Technology 2017;12:1007–15. https://doi.org/10.5370/JEET.2017.12.3.1007.

[48] Yang J, Tushar W, Saha TK, Alam MR, Li Y. Prosumer-Driven Voltage Regulation via Coordinated Real and Reactive Power Control. IEEE Trans Smart Grid 2022;13:1441–52. https://doi.org/10.1109/TSG.2021.3125339.

[49] Merabet A, Labib L, Ghias AMYM, Aldurra A, Debbouza M. Dual-mode operation based second-order sliding mode control for grid-connected solar photovoltaic energy system. International Journal of Electrical Power & Energy Systems 2019;111:459–74. https://doi.org/10.1016/J.IJEPES.2019.04.036.

[50] Patel S, Ahmed M, Kamalasadan S. A Novel Energy Storage-Based Net-Load Smoothing and Shifting Architecture for High Amount of Photovoltaics Integrated Power Distribution System. IEEE Trans Ind Appl 2020;56:3090–9. https://doi.org/10.1109/TIA.2020.2970380.

[51] Olaszi BD, Ladanyi J. Comparison of different discharge strategies of grid-connected residential PV systems with energy storage in perspective of optimal battery energy storage system sizing. Renewable and Sustainable Energy Reviews 2017;75:710–8. https://doi.org/10.1016/J.RSER.2016.11.046.

[52] Krishnan A V., Kumar NS. REAL-TIME SIMULATION ANALYSIS OF LM ALGORITHM-BASED NN FOR THE CONTROL OF VSC IN GRID CONNECTED PV-DIESEL MICROGRID USING OP4500 RT-LAB SIMULATOR, 1-7. International Journal of Power and Energy Systems 2022 2022;42. https://doi.org/10.2316/J.2022.203-0419.

[53] Karimi M, Mokhlis H, Naidu K, Uddin S, Bakar AHA. Photovoltaic penetration issues and impacts in distribution network - A review. Renewable and Sustainable Energy Reviews 2016;53:594–605. https://doi.org/10.1016/j.rser.2015.08.042.

[54] Belouda M, Hajjaji M, Sliti H, Mami A. Bi-objective optimization of a standalone hybrid PV–Wind–battery system generation in a remote area in Tunisia. Sustainable Energy, Grids and Networks 2018;16:315–26. https://doi.org/10.1016/j.segan.2018.09.005.

[55] Arévalo P, Benavides D, Lata-García J, Jurado F. Energy control and size optimization of a hybrid system (photovoltaic-hidrokinetic) using various storage technologies. Sustain Cities Soc 2020;52:101773. https://doi.org/10.1016/j.scs.2019.101773.

[56] Panhwar IH, Ahmed K, Seyedmahmoudian M, Stojcevski A, Horan B, Mekhilef S, et al. Mitigating Power Fluctuations for Energy Storage in Wind Energy Conversion System Using Supercapacitors. IEEE Access 2020;8:189747–60. https://doi.org/10.1109/access.2020.3031446.

[57] González LG, Chacon R, Delgado B, Benavides D, Espinoza J. Study of Energy Compensation Techniques in Photovoltaic Solar Systems with the Use of Supercapacitors in Low-Voltage Networks. Energies (Basel) 2020;13:3755. https://doi.org/10.3390/en13153755.

[58] The CellCube system - Cellcube n.d. https://www.cellcube.com/the-cellcube-system/ (accessed April 2, 2023).

[59] D'Agostino R, Baumann L, Damiano A, Boggasch E. A Vanadium-Redox-Flow-Battery Model for Evaluation of Distributed Storage Implementation in Residential Energy Systems. IEEE Transactions on Energy Conversion 2015;30:421–30. https://doi.org/10.1109/TEC.2014.2369437.

[60] Chahwan J, Abbey C, Joos G. VRB modelling for the study of output terminal voltages, internal losses and performance. 2007 IEEE Canada Electrical Power Conference, EPC 2007 2007:387–92. https://doi.org/10.1109/EPC.2007.4520363.

[61] Sukkar T, Skyllas-Kazacos M. Water transfer behaviour across cation exchange membranes in the vanadium redox battery. J Memb Sci 2003;222:235–47. https://doi.org/10.1016/S0376-7388(03)00309-0.

[62] Espinoza JL, Gonzalez LG, Sempertegui R. Micro grid laboratory as a tool for research on non-conventional energy sources in Ecuador. 2017 IEEE International Autumn Meeting on Power, Electronics and Computing, ROPEC 2017 2018;2018-Janua:1–7. https://doi.org/10.1109/ROPEC.2017.8261615.

[63] Benavides D, Arévalo P, Villa-Ávila E, Aguado JA, Jurado F. Predictive power fluctuation mitigation in grid-connected PV systems with rapid response to EV charging stations. J Energy Storage 2024;86:111230. https://doi.org/10.1016/J.EST.2024.111230.

[64] Wood M, Ogliari E, Nespoli A, Simpkins T, Leva S. Day Ahead Electric Load Forecast: A Comprehensive LSTM-EMD Methodology and Several Diverse Case Studies. Forecasting 2023;5:297–314. https://doi.org/10.3390/FORECAST5010016.

[65] Liang H, Wu J, Zhang H, Yang J. Two-Stage Short-Term Power Load Forecasting Based on RFECV Feature Selection Algorithm and a TCN–ECA–LSTM Neural Network. Energies (Basel) 2023;16. https://doi.org/10.3390/EN16041925.

[66] Sharma M, Mittal N, Mishra A, Gupta A. Machine Learning-Based Electricity Load Forecast for the Agriculture Sector. International Journal of Software Innovation 2023;11. https://doi.org/10.4018/IJSI.315735.

[67] Liu Q, Cao J, Zhang J, Zhong Y, Ba T, Zhang Y. Short-Term Power Load Forecasting in FGSM-Bi-LSTM Networks Based on Empirical Wavelet Transform. IEEE Access 2023;11:105057–68. https://doi.org/10.1109/ACCESS.2023.3316516.

[68] Zhang Z, Dong Y, Hong WC. Long Short-Term Memory-Based Twin Support Vector Regression for Probabilistic Load Forecasting. IEEE Trans Neural Netw Learn Syst 2023. https://doi.org/10.1109/TNNLS.2023.3335355.

[69] Zhang S, Chen R, Cao J, Tan J. A CNN and LSTM-based multi-task learning architecture for short and medium-term electricity load forecasting. Electric Power Systems Research 2023;222. https://doi.org/10.1016/J.EPSR.2023.109507.

[70] Jung JH. Power hardware-in-the-loop simulation (PHILS) of photovoltaic power generation using real-time simulation techniques and power interfaces. J Power Sources 2015;285:137–45. https://doi.org/10.1016/J.JPOWSOUR.2015.03.052.